The Astrophysical Journal, 670:1504–1509, 2007 December 1

LABORATORY MEASUREMENTS OF 3 → 2 X-RAY LINE RATIOS OF F-LIKE Fe XVIII AND Ni XX

M. F. Gu,[1] H. Chen,[1] G. V. Brown,[1] P. Beiersdorfer,[1] and S. M. Kahn[2]

Received 2007 March 12; accepted 2007 August 3

ABSTRACT

The intensity ratios of 3 → 2 emission lines of Fe XVIII and Ni XX were measured on the Livermore electron beam ion trap EBIT-I with a flat-field grating spectrometer. The results are compared with distorted-wave (DW) calculations obtained with the Flexible Atomic Code and recent close-coupling calculations using the ***R***-matrix code. The measured 2*p*–3*s*/2*p*–3*d* ratios are about 20%–40% higher than the theoretical values. When more extended configuration interaction is included in the DW theory, the agreement with the measurements improved slightly. At the beam energies of these measurements, no significant resonance contribution is expected to be present, and so the discrepancies represent the uncertainties in the direct excitation cross sections.

Subject headings: atomic data — atomic processes — line: formation — X-rays: general

1. INTRODUCTION

The spectroscopy of the Fe L-shell X-ray emission is an important diagnostic tool for electron temperature and density, and iron abundances. The emission lines are dominated by 3 → 2 transitions from Fe XVII–XXIV. Although theoretical predictions of these line intensities have improved substantially over recent years, they still disagree significantly with laboratory measurements and astrophysical observations for many key transitions. One of the most serious issues in existing theoretical models is that calculations have not been able to reproduce the observed Ne-like Fe XVII spectrum with an accuracy comparable to the statistical uncertainties of many grating observations obtained with *Chandra* and *XMM-Newton* (Behar et al. 2001; Xu et al. 2002), and earlier crystal spectrometer data from the Sun (Parkinson 1975; McKenzie et al. 1980; Phillips et al. 1982). There are two problems with the Fe XVII line ratios. One involves the relative intensity of two 2*p*–3*d* transitions located near 15 Å, commonly labeled 3C and 3D. Theoretical predictions of the 3C/3D ratio have been consistently larger than astrophysical observations, leading to speculations that opacity effects may have suppressed the stronger 3C line (Rugge & McKenzie 1985; Saba et al. 1999). However, laboratory astrophysics measurements with electron beam ion traps (EBIT) at the Lawrence Livermore National Laboratory (LLNL) and tokamaks at the Princeton Plasma Physics Laboratory have demonstrated that this low 3C/3D ratio is also obtained in optically thin plasmas (Brown et al. 1998, 2001b, 2001a; Beiersdorfer et al. 2001, 2004). Moreover, it has also been shown that this ratio is further reduced by line blending with Fe XVI satellite transitions (Brown et al. 2001b; Behar et al. 2001; Brickhouse & Schmelz 2006). Another problem with the Fe XVII spectrum concerns the ratio of the 2*p*–3*s* (near 17 Å) to 2*p*–3*d* line intensities. This ratio is found to be significantly larger in astrophysical observations than most theoretical predictions (Phillips et al. 1999; Beiersdorfer et al. 2004). Because 2*p*–3*s* transitions are affected by radiative cascades and resonance contributions to a larger degree, it has been assumed that the models of their intensities are more vulnerable to large uncertainties. However, LLNL EBIT measurements have again shown that this ratio is larger than theoretical calculations even in resonance-free energy regions (Beiersdorfer et al. 2002). Brown et al. (2006) have recently measured the formation cross sections of 3C and 3D lines of Fe XVII by normalization to radiative recombination (RR) emission using the Goddard Space Flight Center X-ray microcalorimeter and the LLNL EBIT-I electron beam ion trap, and demonstrated that theoretical cross sections of the 3C line have the largest error, and are larger than measured.

Similar problems with the 2*p*–3*s*/2*p*–3*d* line ratios of F-like Fe XVIII have also been observed in the *XMM-Newton* data for NGC 4636 (Xu et al. 2002). However, the recent cross section measurements of the strongest 2*p*–3*d* lines of Fe XVIII (Chen et al. 2006) indicate that the disagreement with the theory is not as large as for the 3C line of Fe XVII. Unfortunately, the spectrometer used in that measurement did not cover the strong 2*p*–3*s* transitions at wavelengths larger than 15.6 Å. Witthoeft et al. (2006) presented ***R***-matrix calculations of Fe XVIII line intensities, which are in better agreement with the *Chandra* observation of the Capella spectrum than previous distorted-wave (DW) theories without resonance contributions. However, significant discrepancies exist for the 2*p*–3*s* line intensities between the new ***R***-matrix theory and the Capella observation for Fe XVIII. For example, the observed intensity of the 16.008 Å line is significantly larger than the $n = 4$ and $n = 3$ ***R***-matrix results calculated at a temperature of $10^{6.8}$ K, which is more appropriate for the Capella corona than the lower temperature of $10^{6.6}$ K. In this paper, we present the measurements of line ratios of all significant 3 → 2 transitions of Fe XVIII and its isoelectronic equivalent, Ni XX, at electron energies close to the ionization thresholds of the respective ions, where no resonant processes are expected to contribute to the line intensities. In § 2, we discuss the details of our measurements and data analysis. The results and comparisons with various theoretical predictions are presented in § 3, and § 4 gives a brief summary.

2. MEASUREMENT AND ANALYSIS

The experiment was carried out on the EBIT-I electron beam ion trap of the Lawrence Livermore National Laboratory using a high-resolution flat-field grating spectrometer. The details of the LLNL EBITs can be found elsewhere (Levine et al. 1988; Beiersdorfer 2003). The calibration and performance of the grating spectrometer are described in Beiersdorfer et al. (2004). The beam energy was set at 1.4 keV for the Fe XVIII measurement and

[1] Lawrence Livermore National Laboratory, 7000 East Avenue, Livermore, CA 94550.
[2] Department of Physics, Stanford University, Stanford, CA 94305.

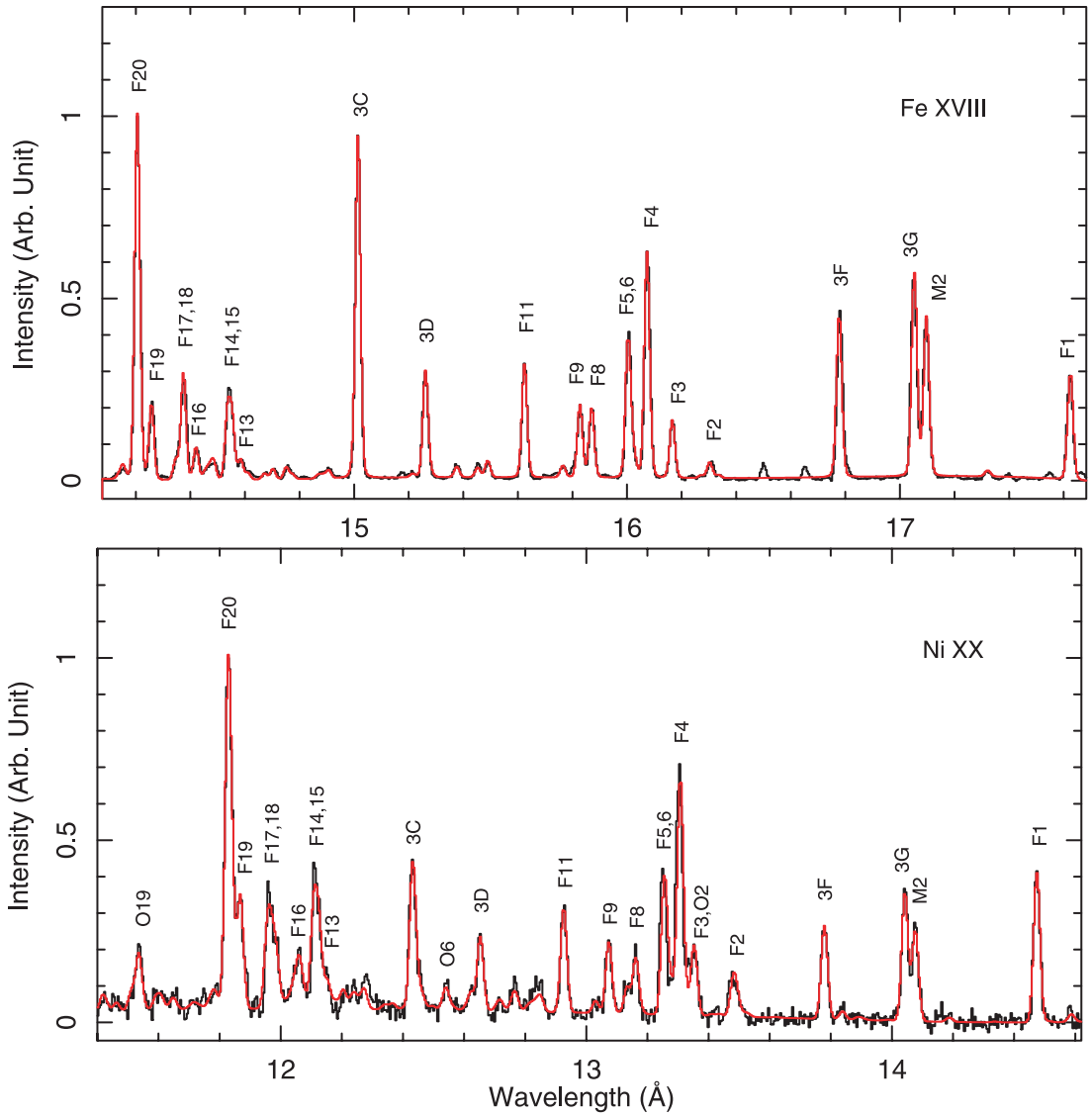

FIG. 1.—Measured spectra and model fits of Fe XVIII and Ni XX lines. Black and red traces are the data and models, respectively. The model fits are the results of the second step in our analysis method as described in § 2. The lines labeled as 3C, 3D, 3F, 3G, and M2 are Ne-like transitions.

1.7 keV for the Ni XX measurement, after accounting for the space charge potential corrections. These energies are slightly above the ionization potentials of Fe XVIII and Ni XX. They were chosen to maximize the populations of the two ions under study and minimize those of the neighboring charge states. Iron and nickel were injected in the form of $Fe(CO)_5$ and $(C_5H_5)_2Ni$, i.e., iron pentacarbonyl and bis(cyclopentadienyl) nickel, respectively, using a differential gas injection system. The electron density in the trap was $<10^{12}$ cm^{-3}, and considered to be in the low-density coronal limit for Fe XVIII and Ni XX lines, i.e., only excitations from ground state and radiative cascades need to be considered in line formation.

The recorded spectra of iron and nickel are shown as the black traces in Figure 1. The spectra are dominated by the Ne-like and F-like ions. The line labels shown in Figure 1 are those used in Brown et al. (1998, 2002) for iron ions, and Gu et al. (2007) for nickel ions. The identification of lower and upper levels of individual transitions are shown in Tables 1 and 2 for Fe XVIII and Ni XX lines, respectively. The configuration labels listed by Brown et al. (2002) and Gu et al. (2007) sometimes give only the main component when the lines contain blended features. In our analysis, such blends are fully taken into account as described below, and all significant contributions to each line are given in the two tables. In our analysis and comparison between measured wavelengths and the recent MBPT calculations of Gu (2005), we found that the identification of the line at 16.045(10) Å with the transition $2s^2 2p_{1/2} 2p_{3/2}^3 3s (J = 1/2) \rightarrow 2s^2 2p_{1/2} 2p_{3/2}^4 (J = 1/2)$ by Brown et al. (2002) is incorrect. Brown et al.'s identification was based on a comparison to a wavelength predicted by HULLAC to be 16.044 Å. However, the MBPT results of Gu (2005) give a wavelength of 16.024 Å for that transition. The 16.024 line in our present measurement blends with the stronger line measured at 16.004(2) Å, and is too weak relative to the predicted line at 16.003 Å to cause significant broadening or wavelength shift. Based on the agreement found between the MBPT and measurements for other Fe XVIII lines, the line measured at 16.045(10) Å by Brown et al. (2002) is likely an unidentified background line. Similarly, the F7 line measured by Brown et al. (2002) at 15.931 Å is also likely a background transition. In Brown et al. (2002) the transition $2s^2 2p_{1/2} 2p_{3/2}^3 3s (J = 3/2) \rightarrow 2s^2 2p_{1/2} 2p_{3/2}^4 (J = 1/2)$ was assigned to this line based on its HULLAC wavelength of 15.901 Å. The MBPT calculation, however, predicts the wavelength to be

TABLE 1

IDENTIFICATIONS OF Fe XVIII X-RAY LINES MEASURED IN THE PRESENT WORK AND IDENTIFIED IN BROWN ET AL. (2002) AND DEL ZANNA (2006)

	BROWN ET AL. (2002)[a]			DEL ZANNA (2006)[b]			GU (2005)[c]
Label	Lower (J)	Upper (J)	λ (Å)	Lower	Upper	λ (Å)	λ (Å)
F1	$2s2p^6\left(\frac{1}{2}\right)$	$2s^22p_{1/2}2p_{3/2}^3 3p_{1/2}\left(\frac{3}{2}\right)$	17.623(3)	$2s2p^6(^2S_{1/2})$	$2s^22p^43p(^2P_{3/2})$	17.622(4)	17.625
F2[d]	$2s2p^6\left(\frac{1}{2}\right)$	$2s2p_{1/2}^2 2p_{3/2}^3 3s\left(\frac{3}{2}\right)$	16.320(5)	$2s2p^6(^2S_{1/2})$	$2s2p^53s(^4P_{3/2})$	16.306(5)	16.302
F3	$2s2p^6\left(\frac{1}{2}\right)$	$2s2p_{1/2}2p_{3/2}^4 3s\left(\frac{3}{2}\right)$	16.159(5)	$2s2p^6(^2S_{1/2})$	$2s2p^53s(^2P_{3/2})$	16.166(4)	16.165
F4	$2s^22p_{1/2}^2 2p_{3/2}^3\left(\frac{3}{2}\right)$	$2s^22p_{1/2}^2 2p_{3/2}^2 3s\left(\frac{5}{2}\right)$	16.071(3)	$2s^22p^5(^2P_{3/2})$	$2s^22p^43s(^4P_{5/2})$	16.072(4)	16.072
F5[e]	$2s^22p_{1/2}2p_{3/2}^4\left(\frac{1}{2}\right)$	$2s^22p_{1/2}2p_{3/2}^3 3s\left(\frac{1}{2}\right)$	16.045(10)	$2s^22p^5(^2P_{1/2})$	$2s^22p^43s(^2P_{1/2})$	16.026(4)	16.024
F6	$2s^22p_{1/2}^2 2p_{3/2}^3\left(\frac{3}{2}\right)$	$2s^22p_{1/2}^2 2p_{3/2}^2 3s\left(\frac{3}{2}\right)$	16.004(2)	$2s^22p^5(^2P_{3/2})$	$2s^22p^43s(^2P_{3/2})$	16.005(5)	16.003
F8	$2s^22p_{1/2}2p_{3/2}^4\left(\frac{1}{2}\right)$	$2s^22p_{1/2}2p_{3/2}^3 3s\left(\frac{3}{2}\right)$	15.870(3)	$2s^22p^5(^2P_{1/2})$	$2s^22p^43s(^2D_{3/2})$	15.870(4)	15.869
	$2s^22p_{1/2}^2 2p_{3/2}^3\left(\frac{3}{2}\right)$[f]	$2s^22p_{1/2}^2 2p_{3/2}^2 3s\left(\frac{1}{2}\right)$	...	$2s^22p^5(^2P_{3/2})$	$2s^22p^43s(^4P_{1/2})$	...	15.871
F9	$2s^22p_{1/2}^2 2p_{3/2}^3\left(\frac{3}{2}\right)$	$2s^22p_{1/2}2p_{3/2}^3 3s\left(\frac{3}{2}\right)$	15.824(3)	$2s^22p^5(^2P_{3/2})$	$2s^22p^43s(^4P_{3/2})$	15.828(4)	15.827
F11	$2s^22p_{1/2}^2 2p_{3/2}^3\left(\frac{3}{2}\right)$	$2s^22p_{1/2}2p_{3/2}^3 3s\left(\frac{5}{2}\right)$	15.625(3)	$2s^22p^5(^2P_{3/2})$	$2s^22p^43s(^2D_{5/2})$	15.622(3)	15.624
F13[d]	$2s^2p_{1/2}^2 2p_{3/2}^3\left(\frac{3}{2}\right)$	$2s^22p_{1/2}^2 2p_{3/2}^2 3d_{5/2}\left(\frac{1}{2}\right)$	14.616(10)	$2s^22p^5(^2P_{3/2})$	$2s^22p^43d(^4P_{1/2})$	14.580(2)	14.584
F14[d]	$2s^22p_{1/2}^2 2p_{3/2}^3\left(\frac{3}{2}\right)$	$2s^22p_{1/2}^2 2p_{3/2}^2 3d_{5/2}\left(\frac{3}{2}\right)$	14.571(11)	$2s^22p^5(^2P_{3/2})$	$2s^22p^43d(^4P_{3/2})$	14.551(4)	14.552
F15	$2s^2p_{1/2}^2 2p_{3/2}^3\left(\frac{3}{2}\right)$	$2s^22p_{1/2}^2 2p_{3/2}^2 3d_{5/2}\left(\frac{5}{2}\right)$	14.534(3)	$2s^22p^5(^2P_{3/2})$	$2s^22p^43d(^4F_{5/2})$	14.537(2)	14.536
F16[g]	$2s^22p_{1/2}2p_{3/2}^4\left(\frac{1}{2}\right)$	$2s^22p_{1/2}2p_{3/2}^3 3d_{5/2}\left(\frac{3}{2}\right)$	14.425(9)	$2s^22p^5(^2P_{1/2})$	$2s^22p^43d(^2P_{3/2})$	14.419(2)	14.419
	$2s^22p_{1/2}^2 2p_{3/2}^3\left(\frac{3}{2}\right)$	$2s^22p_{1/2}2p_{3/2}^3 3d_{5/2}\left(\frac{5}{2}\right)$	...	$2s^22p^5(^2P_{3/2})$	$2s^22p^43d(^4P_{5/2})$	...	14.421
F17	$2s^22p_{1/2}^2 2p_{3/2}^3\left(\frac{3}{2}\right)$	$2s^22p_{1/2}2p_{3/2}^3 3d_{3/2}\left(\frac{5}{2}\right)$	14.373(6)	$2s^22p^5(^2P_{3/2})$	$2s^22p^43d(^2D_{5/2})$	14.373(2)	14.374
F18[g]	$2s^22p_{1/2}2p_{3/2}^4\left(\frac{1}{2}\right)$	$2s^22p_{1/2}2p_{3/2}^3 3d_{3/2}\left(\frac{3}{2}\right)$	14.343(10)	$2s^22p^5(^2P_{1/2})$	$2s^22p^43d(^2D_{3/2})$	14.353(8)	14.361
	$2s^22p_{1/2}2p_{3/2}^4\left(\frac{1}{2}\right)$	$2s^22p_{1/2}2p_{3/2}^3 3d_{5/2}\left(\frac{1}{2}\right)$	...	$2s^22p^5(^2P_{1/2})$	$2s^22p^43d(^2P_{1/2})$	14.344(6)	14.346
F19	$2s^22p_{1/2}^2 2p_{3/2}^3\left(\frac{3}{2}\right)$	$2s^22p_{1/2}2p_{3/2}^3 3d_{3/2}\left(\frac{1}{2}\right)$	14.256(5)	$2s^22p^5(^2P_{3/2})$	$2s^22p^43d(^2S_{1/2})$	14.258(2)	14.257
	$2s^22p_{1/2}^2 2p_{3/2}^3\left(\frac{3}{2}\right)$	$2s^22p_{1/2}2p_{3/2}^3 3d_{5/2}\left(\frac{5}{2}\right)$	...	$2s^22p^5(^2P_{3/2})$	$2s^22p^43d(^2F_{5/2})$	...	14.257
F20	$2s^22p_{1/2}^2 2p_{3/2}\left(\frac{3}{2}\right)$	$2s^22p_{1/2}2p_{3/2}^3 3d_{3/2}\left(\frac{5}{2}\right)$	14.208(3)	$2s^22p^5(^2P_{3/2})$	$2s^22p^43d(^2D_{5/2})$	14.204(2)	14.203
	$2s^22p_{1/2}^2 2p_{3/2}\left(\frac{3}{2}\right)$	$2s^22p_{1/2}2p_{3/2}^3 3d_{5/2}\left(\frac{3}{2}\right)$	...	$2s^22p^5(^2P_{3/2})$	$2s^22p^43d(^2P_{3/2})$	14.209(2)	14.209

[a] Identifications and wavelengths of Brown et al. (2002). Numbers in parentheses in the wavelengths columns are uncertainties in mÅ. Configuration labels are in *jj*-coupling notation.

[b] Identifications and wavelengths of Del Zanna (2006). Configuration labels are in *LS*-coupling notation.

[c] Many-body perturbation theoretical wavelengths of Gu (2005).

[d] F2, F13, and F14 are relatively weak lines, and F14 blends with F15. The wavelengths measured in Brown et al. (2002) have large uncertainties, and deviate from the results of Del Zanna (2006) by about 2–3 σ error bars.

[e] Brown et al. (2002) misidentified this transition as a non-iron background line at 16.045 Å; see text for explanation.

[f] Brown et al. (2002) misidentified this transition as a non-iron background line at 15.931(8) Å, and labeled F7; see text for explanation.

[g] Brown et al. (2002) gave only one transition each for F16 and F18.

15.871 Å. In fact, of the lines in the F8 blend given in Table 1, HULLAC predicts the $J = 1/2 \rightarrow J = 3/2$ line to have a larger wavelength than the $J = 3/2 \rightarrow J = 1/2$ line, while MBPT predicts the wavelength of the $J = 3/2 \rightarrow J = 1/2$ to be larger. We adopt the MBPT theory predictions as correct based on the good agreement found for the other transitions, and the fact that, in the Ni XX spectrum, where the X-ray lines from the same transitions are resolved, the agreement between the MBPT and the EBIT measurements is excellent.

Del Zanna (2006) reevaluated the Fe XVIII line identifications using laser-produced laboratory spectra, atomic structure calculations with SUPERSTUCTURE (Eissner et al. 1974), and ***R***-matrix collisional excitation calculations of Witthoeft et al. (2006). The identifications and recommended wavelengths of Del Zanna (2006) are also shown in Table 1 for comparison with those of Brown et al. (2002). Apart from the two misidentified transitions mentioned above and the weak transitions F2, F13, and F14, the measurements of Brown et al. (2002) and Del Zanna (2006) agree with each other. In our analysis, we adopt the measured wavelengths with smallest uncertainties from either source for Fe XVIII and the measured values of Gu et al. (2007) for Ni XX to establish the wavelength scales. Tables 1 and 2 also list the many-body perturbation theoretical wavelengths of Gu (2005), which agree with the best measurements for both Fe XVIII and Ni XX. In the spectral fitting procedure described below, the wavelengths of numerous weak lines, which have not been measured but contribute to the spectra, are taken from these calculations.

Some of the measured Fe XVIII and Ni XX lines have multiple components, and many have contributions from several weak lines. In the case of the nickel measurement, O-like transitions may also contribute to the Ni XX line intensities. To accurately account for these blends, we use a two-step fitting procedure to extract F-like line intensities. In the first step, we construct theoretical models using the Flexible Atomic Code (FAC; Gu 2003) for Ne-like, F-like, and O-like ions under monoenergetic electron impact excitation conditions. In these calculations, we include configuration interaction effects within all $n = 2$ and $n = 3$ configurations of respective ions in the atomic structure calculation. Collisional excitation cross sections are obtained in the DW approximation. Because the photons are detected in the direction perpendicular to the electron beam, an anisotropic correction factor is also calculated and included in the analysis. The correction factors are typically less than 10%, and uncertainties associated with them are assumed to be negligible. The measured spectra are then fitted with theoretical models adjusting only the populations of Ne-like, F-like, and O-like ions. The line profile is assumed to be Gaussian, and the width is allowed to vary linearly as a function of the wavelength. For the iron spectra, no O-like lines are detected, and the O-like abundance is fixed at zero. In the second step, we fix the ion abundances derived in the first

TABLE 2

IDENTIFICATIONS OF Ni XX X-RAY LINES MEASURED IN THE PRESENT WORK AND IDENTIFIED IN GU ET AL. (2007)

	GU ET AL. (2007)[a]			GU (2005)[b]
Label	Lower (J)	Upper (J)	λ (Å)	λ (Å)
F1	$2s2p^6(\frac{1}{2})$	$2s^22p_{1/2}2p_{3/2}^33p_{1/2}(\frac{3}{2})$	14.470(5)	14.475
F2	$2s2p^6(\frac{1}{2})$	$2s2p_{1/2}^22p_{3/2}^33s(\frac{3}{2})$	13.483(6)	13.480
F3	$2s2p^6(\frac{1}{2})$	$2s2p_{1/2}^22p_{3/2}^33s(\frac{3}{2})$	13.361(5)	13.361
F4	$2s^22p_{1/2}^22p_{3/2}^3(\frac{3}{2})$	$2s^22p_{1/2}^22p_{3/2}^23s(\frac{5}{2})$	13.310(3)	13.308
F5[c]	$2s^22p_{1/2}2p_{3/2}^4(\frac{1}{2})$	$2s^22p_{1/2}2p_{3/2}^33s(\frac{1}{2})$	...	13.281
F6	$2s^22p_{1/2}^22p_{3/2}^3(\frac{3}{2})$	$2s^22p_{1/2}^22p_{3/2}^23s(\frac{3}{2})$	13.259(3)	13.256
F8	$2s^22p_{1/2}2p_{3/2}^4(\frac{1}{2})$	$2s^22p_{1/2}2p_{3/2}^33s(\frac{3}{2})$	13.165(4)	13.162
	$2s^22p_{1/2}^22p_{3/2}^3(\frac{3}{2})$	$2s^22p_{1/2}^22p_{3/2}^23s(\frac{1}{2})$	13.135(5)	13.133
F9	$2s^22p_{1/2}^22p_{3/2}^3(\frac{3}{2})$	$2s^22p_{1/2}2p_{3/2}^33s(\frac{3}{2})$	13.078(4)	13.074
F11	$2s^22p_{1/2}^22p_{3/2}^3(\frac{3}{2})$	$2s^22p_{1/2}2p_{3/2}^33s(\frac{5}{2})$	12.930(4)	12.926
F13[c]	$2s^2p_{1/2}^22p_{3/2}^3(\frac{3}{2})$	$2s^22p_{1/2}^22p_{3/2}^23d_{5/2}(\frac{1}{2})$	...	12.153
F14[d]	$2s^22p_{1/2}^22p_{3/2}^3(\frac{3}{2})$	$2s^22p_{1/2}^22p_{3/2}^23d_52(\frac{3}{2})$	12.115(4)	12.125
F15[d]	$2s^2p_{1/2}^22p_{3/2}^3(\frac{3}{2})$	$2s^22p_{1/2}^22p_{3/2}^23d_{5/2}(\frac{5}{2})$	12.115(4)	12.108
F16[e]	$2s^22p_{1/2}2p_{3/2}^4(\frac{1}{2})$	$2s^22p_{1/2}2p_{3/2}^33d_{3/2}(\frac{3}{2})$	12.059(6)	12.039
	$2s^22p_{1/2}^22p_{3/2}^3(\frac{3}{2})$	$2s^22p_{1/2}^22p_{3/2}^23d_{5/2}(\frac{5}{2})$	...	12.055
	$2s^22p_{1/2}^22p_{3/2}^3(\frac{3}{2})$	$2s^22p_{1/2}^22p_{3/2}^23d_{3/2}(\frac{3}{2})$	...	12.061
F17	$2s^22p_{1/2}^22p_{3/2}^3(\frac{3}{2})$	$2s^22p_{1/2}2p_{3/2}^33d_{3/2}(\frac{5}{2})$	11.960(4)	11.956
F18[c]	$2s^22p_{1/2}2p_{3/2}^4(\frac{1}{2})$	$2s^22p_{1/2}2p_{3/2}^33d_{3/2}(\frac{3}{2})$	...	11.986
	$2s^22p_{1/2}2p_{3/2}^4(\frac{1}{2})$	$2s^22p_{1/2}2p_{3/2}^33d_{5/2}(\frac{1}{2})$	...	11.971
F19	$2s^22p_{1/2}^22p_{3/2}^3(\frac{3}{2})$	$2s^22p_{1/2}2p_{3/2}^33d_{3/2}(\frac{1}{2})$	11.869(5)	11.868
	$2s^22p_{1/2}^22p_{3/2}^3(\frac{3}{2})$	$2s^22p_{1/2}2p_{3/2}^33d_{5/2}(\frac{5}{2})$	...	11.870
F20	$2s^22p_{1/2}^22p_{3/2}(\frac{3}{2})$	$2s^22p_{1/2}2p_{3/2}^33d_{3/2}(\frac{5}{2})$	11.831(3)	11.827
	$2s^22p_{1/2}^22p_{3/2}(\frac{3}{2})$	$2s^22p_{1/2}2p_{3/2}^33d_{3/2}(\frac{3}{2})$	...	11.834

[a] Identifications and wavelengths of Gu et al. (2007). Numbers in parentheses in the wavelength columns are uncertainties in mÅ. Configuration labels are in *jj*-coupling notation.

[b] Many-body perturbation theoretical wavelengths of Gu (2005).

[c] Gu et al. (2007) did not measure the wavelengths of F5, F13, and F18 due to line blending.

[d] F14 and F15 were measured as a single blended feature in Gu et al. (2007).

[e] Gu et al. (2007) gave only two transitions for F16. Unlike iron, the third component in nickel is unresolved.

step but vary the intensities of strong lines of Fe XVIII and Ni XX labeled in Figure 1 during the spectral fitting. For unresolved lines, such as the F5+F6 complex, the F13+F14+F15 complex, and the F17+F18 complex, the intensity ratios of the subcomponents are fixed at the theoretical values, and only the total intensity of the entire complex is reported. The F19 and F20 lines of Fe XVIII are well resolved in our measurement, while the corresponding lines of Ni XX are marginally resolved. In the analysis of nickel data, we also fix the ratio of F19 to F20 according to the FAC calculations. The results of spectral fitting in the second step are shown as red traces in Figure 1. The purpose of this two-step procedure is to determine appropriate contributions of weak lines to the intensities of strong lines under investigation according to theoretical calculations.

3. RESULTS AND DISCUSSIONS

The measured intensities of Fe XVIII and Ni XX lines are normalized relative to the F20 line, and shown in Tables 3 and 4, respectively. The F20 line is the strongest line in the F-like spectra. It comprises two unresolved transitions from $1s^22s^22p^43d$ ($J = 5/2,3/2$) levels to the $1s^22s^22p_{1/2}^22p_{3/2}^3$ ($J = 3/2$) level in the *jj*-coupling notation, or equivalently, in the *LS*-coupling notation, from the $1s^22s^22p^43d$ ($^2D_{5/2}$,$^2P_{3/2}$) levels to the $1s^22s^22p^5$ ($^2P_{3/2}$) level. This line can be considered to be the equivalent of 3C in the Ne-like spectra. The quoted uncertainties are the combination of statistical and systematic errors at the 1 σ confidence level. The systematic uncertainties mainly arise from the spectrometer response, and are assumed to be 10% across the covered wavelength range. This estimate is based on the spectrometer response calibration performed using H-like and He-like Rydberg series of Ne, F, and O ions (Beiersdorfer et al. 2004). The statistical uncertainties are determined according to the total number of X-ray counts in each line complex using Poisson statistics.

The values for "theory A" in Tables 3 and 4 are calculated with the FAC model described in § 2. In order to investigate the effects of configuration interactions on the calculated line ratios,

TABLE 3

COMPARISON OF EXPERIMENTAL AND THEORETICAL LINE RATIOS OF Fe XVIII

Label	Theory A[a]	Theory B[b]	Theory C[c]	Experimental
F20	6.10[d]	5.58[d]	6.00[d]	5.6(8)[d]
F1	0.34	0.32	0.31	0.29(3)
F2	0.042	0.052	0.046	0.043(6)
F3	0.17	0.16	0.15	0.16(2)
F4	0.41	0.48	0.35	0.60(6)
F5, 6	0.31	0.36	0.27	0.44(5)
F8	0.15	0.17	0.12	0.19(2)
F9	0.16	0.17	0.13	0.20(2)
F11	0.25	0.29	0.23	0.30(4)
F13, 14, 15	0.34	0.31	0.38	0.38(4)
F16	0.10	0.10	0.09	0.09(1)
F17, 18	0.37	0.36	0.39	0.33(4)
F19	0.20	0.22	0.19	0.20(2)

[a] Theory with limited configuration interaction, calculated with FAC.

[b] Theory with more extensive configuration interaction, calculated with FAC.

[c] Theory with ***R***-matrix atomic data of Witthoeft et al. (2006).

[d] Line ratios are relative to the intensity (in photon units) of F20. The theoretical values tabulated for F20 are the total effective cross sections for forming this line in units of 10^{-20} cm^2. The experimental formation cross section for F20 is from Chen et al. (2006). Numbers in parentheses for the experimental values are the uncertainties in the last digit.

TABLE 4

COMPARISON OF EXPERIMENTAL AND THEORETICAL LINE RATIOS OF Ni XX

Label	Theory A[a]	Theory B[b]	Experimental
F20	4.5[c]	3.86[c]	...
F1	0.36	0.33	0.36(5)[e]
F2	0.06	0.07	0.08(2)
F3	0.16	0.15	0.13(2)
F4	0.44	0.46	0.58(8)
F5, 6	0.32	0.36	0.42(6)
F8	0.14	0.17	0.20(3)
F9	0.14	0.16	0.18(3)
F11	0.23	0.27	0.26(4)
F13, 14, 15	0.44	0.50	0.55(7)
F16	0.17	0.17	0.17(3)
F17, 18	0.39	0.41	0.40(6)
F19	0.21	0.23	0.21(4)[d]

[a] Theory with limited configuration interaction, calculated with FAC.

[b] Theory with more extensive configuration interaction, calculated with FAC.

[c] Line ratios are relative to the intensity (in photon units) of F20. The theoretical values tabulated for F20 are the total effective cross sections for forming this line in units of 10^{-20} cm^2. Numbers in parentheses for the experimental values are the uncertainties in the last digit.

[d] The F20 and F19 lines of Ni XX are marginally resolved; the ratio of the two lines is fixed at the value predicted by theory A during the spectral fitting.

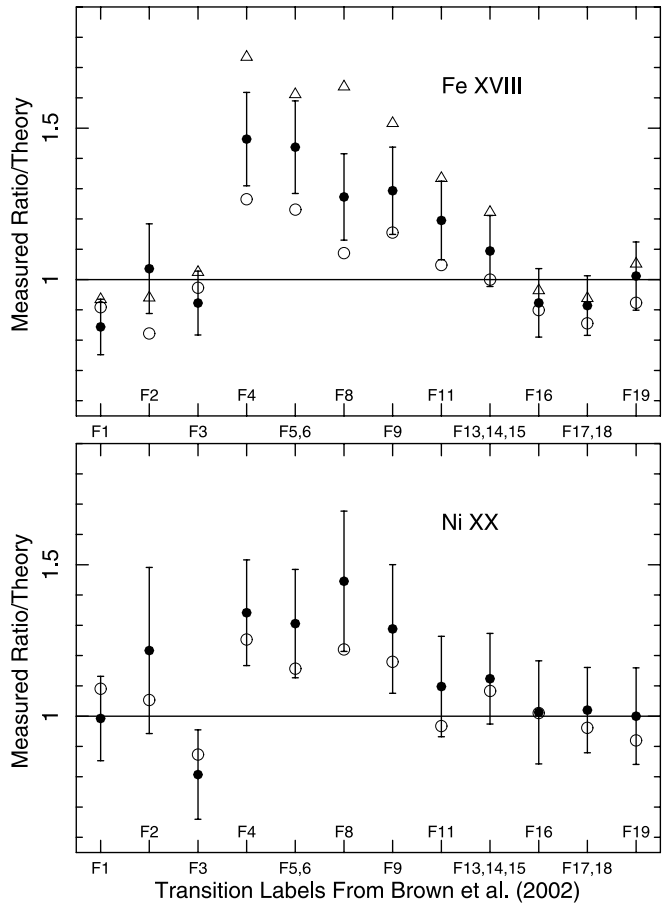

FIG. 2.—Comparison of theoretical and experimental line ratios of Fe XVIII and Ni XX. The filled circles are the ratios of measured to theory A line intensities normalized to that of the F20 line, the open circles are the ratios using theory B, and the open triangles for Fe XVIII are the ratios using theory C.

we performed a larger calculation including all $n \leq 7$ single-excitation configurations, as well as $3l^2$, $3l4l'$, and $4l^2$ doubly excited configurations. The line ratios calculated with this model are referred to as "theory B."

The discrepancies between measured and calculated line ratios are summarized in Figure 2. It is clear that both Fe XVIII and Ni XX data suggest that the theoretical intensities of F4, F5+F6, F8, F9, and F11 lines relative to F20 are underestimated. When compared with theory A values, the discrepancies are largest for F4, F5+F6, and F8, reaching 30%–40%. These lines are all $2p$–$3s$ transitions. Theory B line ratios bring the calculated and measured values into slightly better agreement, but discrepancies remain at the 20% level. On the other hand, the measured intensities of the $2p$–$3d$ transitions, i.e., F13+F14+F15, F16, F17+F18, and F19, relative to that of F20 appear to agree with the theoretical values very well. The measured and calculated ratios for F1, F2, and F3 also agree with each other reasonably well. F1 of Fe XVIII and F3 of Ni XX are slightly overestimated in theory. However, F3 of Ni XX is severely blended with the O-like line, O2, of Ni XXI, which contributes about 30% to the total intensity of the feature. The possible overcorrection of the O2 contribution may partly cause the discrepancy for F3 of Ni XX.

These measurements were carried out at electron energies where no resonant processes are expected to contribute significantly to the line intensities. The discrepancies between theoretical and experimental values therefore reflect the problems in the direct excitation cross sections. Brown et al. (2006) have shown that the $2p$–$3s$/$2p$–$3d$ ratio discrepancies of Fe XVII are largely due to the overestimation of the 3C line cross sections in various theoretical calculations. In Fe XVIII, the measured cross section for F20, i.e., the equivalent of 3C, is $5.6 \pm 0.8 \times 10^{-20}$ cm^2 (Chen et al. 2006) at electron energies of 1.35 and 1.46 keV. The theoretical cross section from theory A is 6.1×10^{-20} cm^2, or about 10% higher than the measured values, and that from theory B is 5.58×10^{-20} cm^2, which agrees very well with the measured values. This indicates that for Fe XVIII, the discrepancies in the $2p$–$3s$/$2p$–$3d$ ratios are mainly due to problems in the line formation cross sections of the $2p$–$3s$ transitions.

Witthoeft et al. (2006) recently computed the Fe XVIII atomic data using the ***R***-matrix theory, including all $n = 3$ and $n = 4$ target states. Resonance excitation was found to play an important role in Fe XVIII line formation. The predicted line ratios were in better agreement with the observed spectra of Capella obtained with the *Chandra* grating spectrometers (Desai et al. 2005) than previous DW calculations without resonances. However, significant discrepancies between the new theory and observations persist for a few transitions. Most notably, the intensities of F4, F5+F6, and F8 relative to F20 are underestimated in theory. Such discrepancies indicate that problems exist in the background collision strengths of ***R***-matrix calculations similar to those in the DW approximation implemented in FAC. We have computed the Fe XVIII line intensities using the atomic data of Witthoeft et al. (2006) for monoenergetic electron collisional excitation conditions at an energy of 1.4 keV, and list the results in Table 3, as "theory C." The effective formation cross section of F20 agrees with the present FAC results very well. The intensities of F4, F5+F6, and F8 are even smaller than the FAC predictions, resulting in slightly worse agreements with the present measurements. This illustrates that the more sophisticated scattering theory of Witthoeft et al. (2006) does not resolve the problem in the direct excitation cross sections.

4. SUMMARY

In summary, we have measured the Fe XVIII and Ni XX line ratios using the Livermore electron beam ion trap EBIT-I and a high-resolution flat-field grating spectrometer, at electron energies where no significant resonant processes are expected. We have shown that the measured $2p$–$3s$/$2d$–$3d$ line ratios are smaller than distorted-wave theoretical calculations using the Flexible Atomic Code (FAC). These discrepancies are attributed to the problems affecting theoretical direct excitation cross sections. It is shown that more sophisticated scattering theory such as the close-coupling approximation implemented in the ***R***-matrix code does not resolve these problems.

The authors wish to thank M. C. Witthoeft for providing the ***R***-matrix atomic data in electronic form. This work was performed under the auspices of the U.S. Department of Energy by Lawrence Livermore National Laboratory under Contract DE-AC52-07NA27344, and supported by NASA Astronomy and Physics Research and Analysis grant NAG5-5419 to Stanford University and LLNL.

REFERENCES

Behar, E., Cottam, J., & Kahn, S. M. 2001, ApJ, 548, 966
Beiersdorfer, P. 2003, ARA&A, 41, 343
Beiersdorfer, P., Bitter, M., von Goeler, S., & Hill, K. W. 2004, ApJ, 610, 616
Beiersdorfer, P., von Goeler, S., Bitter, M., & Thorn, D. B. 2001, Phys. Rev. A, 64, 032705
Beiersdorfer, P., et al. 2002, ApJ, 576, L169
Brickhouse, N. S., & Schmelz, J. T. 2006, ApJ, 636, L53
Brown, G. V., Beiersdorfer, P., Chen, H., Chen, M. H., & Reed, K. J. 2001a, ApJ, 557, L75
Brown, G. V., Beiersdorfer, P., Liedahl, D. A., Widmann, K., & Kahn, S. M. 1998, ApJ, 502, 1015
Brown, G. V., Beiersdorfer, P., Liedahl, D. A., Widmann, K., Kahn, S. M., & Clothiaux, E. J. 2002, ApJS, 140, 589
Brown, G. V., Beiersdorfer, P., & Widmann, K. 2001b, Phys. Rev. A, 63, 032719
Brown, G. V., et al. 2006, Phys. Rev. Lett., 96, 253201
Chen, H., et al. 2006, ApJ, 646, 653
Del Zanna, G. 2006, A&A, 459, 307
Desai, P., et al. 2005, ApJ, 625, L59
Eissner, W., Jones, M., & Nussbaumer, H. 1974, Comput. Phys. Commun., 8, 270
Gu, M. F. 2003, ApJ, 582, 1241
———. 2005, ApJS, 156, 105
Gu, M. F., Beiersdorfer, P., Brown, G. V., Chen, H., Thorn, D. B., & Kahn, S. M. 2007, ApJ, 657, 1172
Levine, M. A., Marrs, R. E., Henderson, J. R., Knapp, D. A., & Schneider, M. B. 1988, Phys. Scr., T22, 157
McKenzie, D. L., Landecker, P. B., Broussard, R. M., Rugge, H. R., Young, R. M., Feldman, U., & Doschek, G. A. 1980, ApJ, 241, 409
Parkinson, J. H. 1975, Sol. Phys., 42, 183
Phillips, K. J. H., Mewe, R., Harra-Murnion, L. K., Kaastra, J. S., Beiersdorfer, P., Brown, G. V., & Liedahl, D. A. 1999, A&AS, 138, 381
Phillips, K. J. H., et al. 1982, ApJ, 256, 774
Rugge, H. R., & McKenzie, D. L. 1985, ApJ, 297, 338
Saba, J. L. R., Schmelz, J. T., Bhatia, A. K., & Strong, K. T. 1999, ApJ, 510, 1064
Witthoeft, M. C., Badnell, N. R., del Zanna, G., Berrington, K. A., & Pelan, J. C. 2006, A&A, 446, 361
Xu, H., et al. 2002, ApJ, 579, 600